

Resonant tunneling in double-quantum-well triple-barrier heterostructures

L. D. Macks, S. A. Brown, R. G. Clark, and R. P. Starrett

National Pulsed Magnet Laboratory, School of Physics, University of New South Wales, Sydney, New South Wales 2052, Australia

M. A. Reed and M. R. Deshpande

Departments of Electrical Engineering and Applied Physics, Yale University, New Haven, Connecticut 06520

C. J. L. Fernando and W. R. Frensley

Eric Jonsson School of Engineering and Computer Science, University of Texas at Dallas, Richardson, Texas 75083

(Received 5 September 1995; revised manuscript received 18 March 1996)

We present a low-temperature (mK) magnetotransport study, using intense pulsed magnetic fields to 50 T, of two double GaAs quantum well, triple AlAs barrier resonant tunneling structures, which demonstrates the critical influence of the second quantum well on the tunneling behavior. We show that charge accumulation in the first well, and thus the overall tunneling characteristic, is controlled by the position of the lowest bound state in the second well, and identify tunneling transitions that are unique to triple-barrier structures. We also demonstrate that the tunneling current is sensitive to integer and fractional quantum Hall effect states, and find that the voltage-tunable accumulation of charge in one of the samples provides an unusual environment for the study of ground states of a two-dimensional electron system. [S0163-1829(96)06431-4]

I. INTRODUCTION

Resonant tunneling processes in semiconductor heterostructures have attracted much interest since the pioneering experiments of Chang, Esaki, and Tsu,¹ due to both the wealth of physical phenomena which can be studied and the significance of potential device applications. Many studies have focused on single-quantum-well, double-barrier resonant tunneling structures (DBRTS's) in which elastic tunneling from the emitter when aligned to bound states in the well leads to sharp current peaks and negative differential resistance (NDR) in the tunneling characteristic.²⁻¹² Intrinsic bistability has been observed in asymmetric DBRTS's and has been related to the accumulation of charge in the well which occurs when the collector barrier is thicker than the emitter barrier, inhibiting current flow out of the well.³⁻⁸ Weaker peaks at higher bias in the tunneling characteristic have been associated with inelastic tunneling processes.⁹⁻¹⁵

Elastic and inelastic tunneling processes have also been identified in triple-barrier resonant tunneling structures (TBRTS's).¹⁶⁻²⁴ Our measurements of two selected GaAs/AlAs TBRTS's at low temperatures and in high magnetic fields demonstrate the critical role played by the second well in determining the overall tunneling characteristic. In sample A, when the emitter and the lowest bound state in the first well are aligned (primary resonance condition), the lowest bound state in the second well is at a higher energy, causing charge to accumulate in the first well. In contrast, at the primary resonance condition in sample B, the lowest bound state in the second well is at lower energy, preventing significant charge accumulation in the first well.

Beyond the primary resonance in sample A, we identify a GaAs longitudinal-optic- (LO-) phonon emission assisted transition from the emitter to a coupled well state. In sample B, we find that the primary resonance is enhanced by a "double resonance": a GaAs LO-phonon emission assisted

transition from the first to the second well, which occurs as a simultaneous complement to the elastic transition from emitter to first well, resulting in a significant increase in the peak tunneling current and current peak to valley ratio.

The tunneling current at the primary resonance in sample A exhibits magneto-oscillations, which correlate with quantum Hall effect (QHE) states associated with a constant two-dimensional (2D) electron density. A maximum at ~ 30 T at mK temperatures, which correlates with Landau-level filling factor $\nu=2/3$, provides evidence for the sensitivity of the tunneling current to fractional QHE (FQHE) states.

We have observed Shubnikov-de Haas (SdH) oscillations in both current and differential conductance allowing the determination of 2D electron densities in the first well and in the emitter in sample A. Sensitivity of the tunneling current to FQHE states, and the presence of a *tunable*, low-density, 2D electron system (2DES) in the first quantum well, makes vertical tunneling in these samples a useful probe of 2D electron ground states in the extreme quantum limit.

II. SAMPLES

Table I details the layer structure of the two samples as grown by molecular-beam epitaxy (MBE). Mesas (ranging from 2- to 64- μm squares on a single chip) were defined by standard photolithography and wet chemical etching. Forward bias is defined as electron flow from the top contact (denoted emitter in Table I) into the wider well (denoted well 1) first.

The band structures of the samples were modeled by a self-consistent Poisson solution, treated in a finite-temperature Thomas-Fermi approximation.²⁵ The application of a bias voltage across the structure causes a relative shift in energy levels which we have calibrated using voltage/energy

TABLE I. Composition details for samples A and B.

	Sample A	Sample B	
Emitter	0.5 μm	0.5 μm	n^+ GaAs Si: $1.5 \times 10^{18} \text{ cm}^{-3}$
	100 \AA	100 \AA	GaAs graded doping
	150 \AA	150 \AA	GaAs undoped
Barrier	40 \AA	40 \AA	AlAs undoped
Well 1	80 \AA	65 \AA	GaAs undoped
Barrier	15 \AA	20 \AA	AlAs undoped
Well 2	50 \AA	50 \AA	GaAs undoped
Barrier	40 \AA	40 \AA	AlAs undoped
	150 \AA	150 \AA	GaAs undoped
	100 \AA	100 \AA	GaAs graded doping
Collector	0.5 μm	0.5 μm	n^+ GaAs Si: $1.5 \times 10^{18} \text{ cm}^{-3}$
Substrate			n^+ GaAs (001)

conversion ratios (α) calculated from the model. The distortion of the potential distribution throughout the structure resulting from the accumulation of charge in the wells is not intrinsically accounted for by the model. Where charge accumulation is significant, we have simulated its effect by explicitly redefining the modeled potential distribution.

III. $I(V)$ MEASUREMENTS

A. In zero magnetic field

In zero magnetic field, the measured tunneling current will comprise two components: elastic peaks due to resonant transmission of electrons between aligned energy states, and an inelastic background signal due to scattering which also exhibits peaks when the energy associated with processes such as plasmon or phonon emission matches the energy difference between final and initial states.

Figure 1 shows the forward bias tunneling characteristics of (a) sample A, 64- μm device and (b) sample B, 64- μm device (solid line) and 2- μm device (dashed line) in zero magnetic field at 1.8 K. The tunneling characteristics are expressed in terms of current density (J) to aid comparison between devices of different sizes. The steplike structure observed in the region of NDR in the 64- μm device for sample B [Fig. 1(b), solid line] is an extrinsic effect arising from oscillations in the circuit current.^{6,26} All subsequent forward bias measurements of sample B were performed on a 2- μm square device resulting in a smooth tunneling characteristic [Fig. 1(b), dashed line].

The left inset to Fig. 1(a) is the modeled conduction-band profile for sample A at the tunneling threshold (arrowed at 150 mV). Modeled wave functions in each well are shown zeroed on the corresponding energy levels. The tunneling current clearly arises from resonant transmission of charge from the emitter to the lowest bound state in well 1 (denoted an $e \rightarrow 1$ transition). Throughout the voltage range of this transition, the lowest bound state in well 2 is at a higher energy and thus appears as part of a thick collector barrier. This results in the accumulation of charge in well 1 (the charge density is measured directly using SdH oscillations in Sec. V). The situation is analogous to charge accumulation in an asymmetric DBRTS.³⁻⁸ The screening effect of the charge accumulated in well 1 causes most of an additional

bias voltage increment to be dropped across well 2, the collector barrier and the collector depletion region, so that the well 1 state is at a higher energy (relative to the emitter) than in the absence of charge accumulation.⁵⁻⁷ This effect is accounted for in the modeled conduction-band profile [right inset to Fig. 1(a)] at the primary resonance peak (arrowed at 305 mV), which shows strong coupling between the lowest bound states in wells 1 and 2 [wave functions in the right inset to Fig. 1(a)]. This provides a mechanism, unique to multiple-quantum-well structures, by which the charge accumulated in well 1 may escape, leading to a redistribution of potential throughout the structure.

The inset to Fig. 1(b) is the modeled conduction-band profile for sample B at the primary resonance peak of the 64- μm device (390 mV) as arrowed. Once again, this peak is

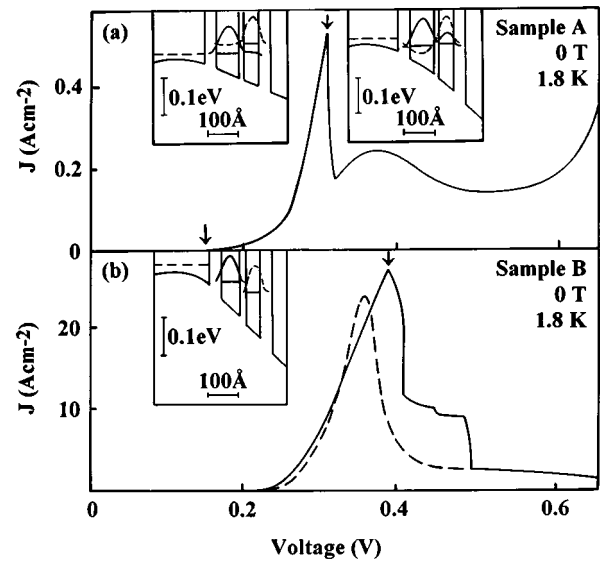


FIG. 1. Forward bias $J(V)$ characteristics for (a) sample A, 64- μm device and (b) sample B, 64- μm device (solid line) and 2- μm device (dashed line) measured at 1.8 K with no applied magnetic field. Insets show modeled conduction-band profiles at the bias positions arrowed on the characteristics. Modeled wave functions for wells 1 and 2 are shown with solid and dashed lines, respectively, zeroed on the corresponding modeled energy level. Horizontal dashed lines mark the emitter Fermi energy.

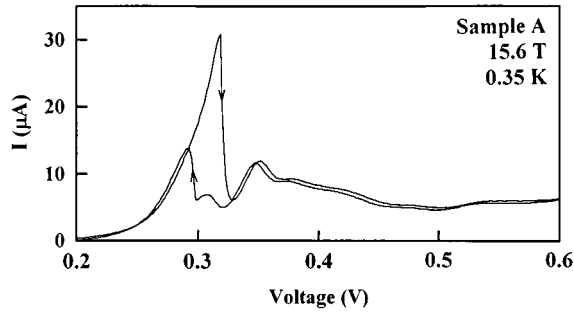


FIG. 2. Forward bias $I(V)$ characteristics from increasing and decreasing fast voltage ramps for sample A at 0.35 K, 15.6 T.

clearly identified as an $e \rightarrow 1$ transition, however, in this sample the lowest bound state in well 2 is at a lower energy than that in well 1 throughout the voltage range of the resonance, providing a path for inelastic transmission out of well 1. SdH measurements indicate no charge accumulation in well 1 in this sample.²⁴ We note that at 390 mV, the modeled energy separation between the lowest bound states in each well is in fact very close to the GaAs LO-phonon energy of 36 meV (Ref. 13) and conclude that the $e \rightarrow 1$ transition is enhanced by a simultaneous GaAs LO-phonon emission assisted $1 \rightarrow 2$ transition. We denote this double resonance $e \rightarrow 1 + 1 \rightarrow 2$ (LO_{GaAs}).²⁷ In this sample, the double resonance leads to a dramatically increased peak tunneling current and current peak to valley ratio. We emphasize that the fundamental difference between samples A and B is the relative energy of the lowest bound states in each well over the bias range of the primary resonance.

B. In strong magnetic fields

The application of a magnetic field perpendicular to the layers leads to quantization of the emitter and quantum-well energies into Landau levels of energy $E_n = (n + \frac{1}{2})\hbar\omega_c$ (where $\omega_c = eB/m^*$ is the cyclotron frequency and $n=0,1,2,\dots$ the Landau-level index). Elastic transitions obey a $\Delta n=0$ selection rule associated with momentum conservation; however, a $\Delta n=0,1,2,\dots$ fan of inelastic inter-Landau-level transitions may be observed in magnetic field.^{10–14} Magnetotransport in resonant tunneling structures is consequently a useful spectroscopic probe of inelastic tunneling processes.

Sample A was mounted in a ^3He cryostat in the bore of a 20-ms, 60-T-pulsed magnet coil for studies with a magnetic field applied parallel to the flow of current. $I(V)$ measurements were made on the 64- μm device using a fast (2 ms) voltage ramp centered on the maximum of the magnetic-field pulse. A full description of this measurement technique has been previously published.¹⁹ Overlap measurements were performed with sample A mounted in a ^4He cryostat/13-T superconducting magnet. Fast voltage ramps in pulsed and steady fields produced identical results. $I(V)$ measurements in steady fields using fast voltage ramps and conventional slow voltage ramps showed differences at high fields. Beyond 8 T, bistability of the primary resonance in forward bias was observed in fast voltage ramps only, as shown, for example, at 15.6 T in Fig. 2. In this region of bistability, an additional peak appears in the decreasing voltage sweep. In

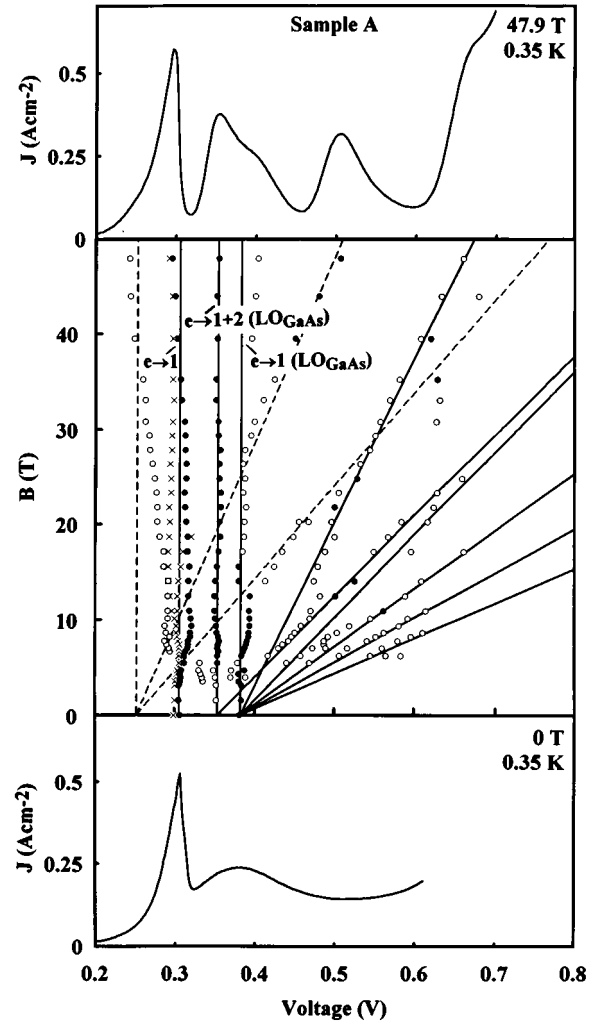


FIG. 3. Sample A resonance peak positions in magnetic field (center) at 0.35 K related to $J(V)$ characteristics at the extreme magnetic fields (top and bottom).

recent measurements of a DBRTS using an active load-line measurement technique to probe the normally inaccessible bistable region, similar structure was observed and identified with plasmon emission assisted tunneling.²⁸

The voltage positions of tunneling current peaks for sample A are detailed in Fig. 3 (center) with examples of measured $J(V)$ data for the extreme fields (0 T, 48 T) shown at the bottom and top. The closed and open circle data in Fig. 3 (center) represent the voltage positions of strong and weak (identified in d^2I/dV^2 only) peaks, respectively, measured from the increasing voltage sweep. For completeness, the voltage positions of the primary resonance peak and additional structure measured from the decreasing voltage sweep (as discussed above) are represented by cross data. All data in the remainder of this paper are drawn from increasing voltage sweeps.

The $e \rightarrow 1$ transition identified in the zero-field data is still the dominant peak at 48 T (Fig. 3, top). In Fig. 3 (center), this transition is marked with a solid vertical line as a guide to the eye. At 0 T, a broad peak is visible beyond the primary resonance (Fig. 3, bottom). As the magnetic field increases, two overlapping peaks are resolved in this voltage range, as seen most clearly at 48 T (Fig. 3, top). These peaks are

marked with solid vertical lines at 350 and 380 mV as guides to the eye in Fig. 3 (center). The peak at 380 mV is identified as a GaAs LO-phonon emission assisted $e \rightarrow 1$ transition, as observed in DBRTS's.⁹⁻¹⁴ Modeling shows alignment and therefore strong coupling of the lowest-energy levels in each well at ~ 350 mV and thus we interpret the peak at 350 mV as an enhancement of the low bias shoulder of the 380-mV peak, due to the increased efficiency of transmission through the structure when the two wells are aligned over a narrow voltage range. This process involving a coupled well state is unique to TBRTS's. The peaks at 350 and 380 mV are both associated with GaAs LO-phonon emission assisted tunneling and are correspondingly labeled $e \rightarrow 1+2$ (LO_{GaAs}) and $e \rightarrow 1$ (LO_{GaAs}), respectively.

For the $e \rightarrow 1$ (LO_{GaAs}) transition, an inter-Landau level fan for $\Delta n = 1-5$ is marked with solid positively sloped lines in Fig. 3 (center) extrapolating back to the $\Delta n = 0$ transition at $B = 0$ T. The measured $\Delta n = 1$ slope of 5.9 mV/T compares well with a modeled slope of $\alpha \hbar \omega_c = 6.2$ mV/T. Another $\Delta n = 1$ inter-Landau level transition with a slope of 11.3 mV/T extrapolates back to the $e \rightarrow 1+2$ (LO_{GaAs}) transition at $B = 0$ T. This represents a transition between the two wells for which the modeled $\Delta n = 1$ slope is 11.7 mV/T.

The $e \rightarrow 1$ (LO_{GaAs}), $\Delta n = 0$ transition should be separated from the $e \rightarrow 1$, $\Delta n = 0$ transition by the GaAs LO-phonon energy of 36 meV.¹³ This would place the $e \rightarrow 1$, $\Delta n = 0$ transition (in the absence of charge accumulation) at ~ 250 mV, as shown by the dashed vertical line in Fig. 3 (center). This assignment is supported by the identification of $e \rightarrow 1$, $\Delta n = 1-2$ transitions (marked with positively sloped dashed lines) at higher bias (and, therefore, unaffected by the charge accumulation), which extrapolate back to ~ 250 mV at $B = 0$ T. The measured $\Delta n = 1$ slope of 5.2 mV/T compares reasonably with the modeled slope of 6.2 mV/T. In this case, the $\Delta n = 0$ selection rule for elastic transitions has been broken, most probably through scattering mechanisms associated with impurities or layer thickness variations.^{14,15}

In sample B, the primary resonance identified in zero field [$e \rightarrow 1+1 \rightarrow 2$ (LO_{GaAs})] remains the dominant feature as the magnetic field is increased to 13 T. Much weaker structure observed at higher bias is attributed to $e \rightarrow 1$ GaAs and AlAs LO-phonon emission assisted transitions.²⁴

IV. VERTICAL TRANSPORT AS A PROBE OF THE QHE

Figure 4 shows striking magneto-oscillations in the peak tunneling current at the primary resonance for sample A in forward bias. The voltage position of the primary resonance peak also oscillates slightly, as can be seen in the deviation of closed circle data from the solid vertical line labeled $e \rightarrow 1$ in Fig. 3 (center). The important feature of Fig. 4 is that the oscillation maxima correlate with QHE states (as marked) associated with a 2D electron density (n_s) of $4.5 \times 10^{11} \text{ cm}^{-2}$. Our identification of a maximum at ~ 30 T in the 0.35-K data (closed circles) with a FQHE state at $\nu = 2/3$ is supported by the observed weakening of this structure at 2 K (open circle data), as the FQHE energy gap is of the order of this temperature difference. The integer filling factor maxima are unchanged at 2 K, as the IQHE energy gaps are, in general, substantially larger.

A $\nu = 1/3$ FQHE state in a 2D emitter has been identified

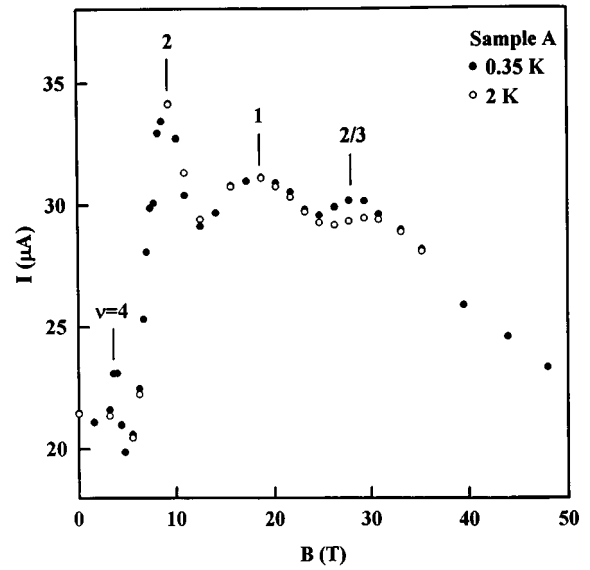


FIG. 4. Peak tunneling current at the primary resonance as a function of magnetic field for sample A at 0.35 K (closed circles) and 2 K (open circles).

in magneto-oscillations of the primary resonance position (but not the peak current) in a DBRTS.²⁹ The location of the 2D charge system that forms the $\nu = 2/3$ FQHE state identified here at precisely the primary resonance is not completely clear, although in the following section magneto-oscillations at lower bias are unambiguously identified with charge in well 1.

V. $I(B)$ AND $g(B)$ MEASUREMENTS AND THE EXTREME QUANTUM LIMIT

SdH oscillations were observed in the tunneling current as magnetic field was swept (using both slowly ramped and ms pulsed fields) at a constant voltage. The differential conductance ($g = dI/dV$) exhibited similar (but stronger) oscillations, measured in slowly ramped magnetic fields using ac lock-in techniques with a small ac modulation of the bias voltage. The 2D electron density (n_s) was calculated from the fundamental frequency of the oscillations,⁵ assuming spin splitting of Landau levels is unresolved, and is shown for sample A in Fig. 5 as a function of forward bias voltage. $I(B)$ measurements in pulsed and steady fields and $g(B)$ measurements in steady fields yielded the same values of n_s .

We identify two branches of $n_s(V)$ data in Fig. 5. The first extrapolates to $n_s = 0$ at the tunneling threshold (150 mV) and reaches a maximum of $n_s = 3 \times 10^{11} \text{ cm}^{-2}$ just beyond the $e \rightarrow 1$ peak (305 mV). We identify these data with electrons accumulated in well 1 and denote this density n_w in Fig. 5. This behavior is similar to that observed in asymmetric DBRTS's.⁵ The second set of data follows a straight line trajectory of smaller gradient, observable only beyond the $e \rightarrow 1$ peak. This is identified with charge in the 2D accumulation layer in the emitter (density denoted n_e in Fig. 5), which forms beyond 305 mV when charge is ejected from the well and the potential throughout the structure is redistributed. The slopes dn_w/dV and dn_e/dV are directly related to the capacitance between the 2D charge and the collector. The decrease in slope between these two data sets is consis-

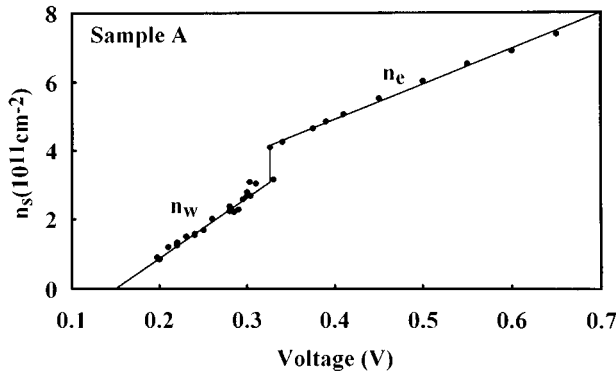


FIG. 5. 2D electron density (n_s) as a function of forward bias voltage for sample A. The lines are best fits to the two branches of the data associated with the charge density in the first well (n_w) and in the 2D accumulation layer in the emitter (n_e).

tent with the 2D charge switching from the well to the emitter beyond the $e \rightarrow 1$ peak. Values of dn_w/dV and dn_e/dV obtained from Fig. 5 agree well with the modeled capacitance of the MBE grown structure. The measurement of n_w confirms our interpretation (in Sec. III) of charge accumulation over the bias range of the primary resonance.

We note from Fig. 5 that by varying the forward bias voltage, the well density can be tuned through a range low enough to access the extreme quantum limit ($\nu \ll 1$) in high magnetic fields. This raises the exciting prospect that vertical transport may provide an alternative to conventional “in-plane” transport measurements for the study of the low-temperature, high-magnetic-field ground states of a 2DES. In particular, we are interested in the effect of magnetically induced Wigner crystallization of the accumulated 2D well charge on the tunneling current. Our experience of measurements in this regime suggests that we need to access the range beyond $\nu = \frac{1}{5}$ at temperatures below 300 mK. We have consequently carried out preliminary measurements on sample A in a $^3\text{He}/^4\text{He}$ dilution refrigerator/17-T superconducting magnet. Figure 6 shows differential conductance oscillations in magnetic field at a constant bias of 230 mV (corresponding to a well density of $1.5 \times 10^{11} \text{ cm}^{-2}$) and temperature of 200 mK. We observe clear minima in $g(B)$ at IQHE states (as marked). In the extreme quantum limit, some structure is apparent in the region around $\nu = \frac{2}{3}$. While these initial measurements are limited by the field range of

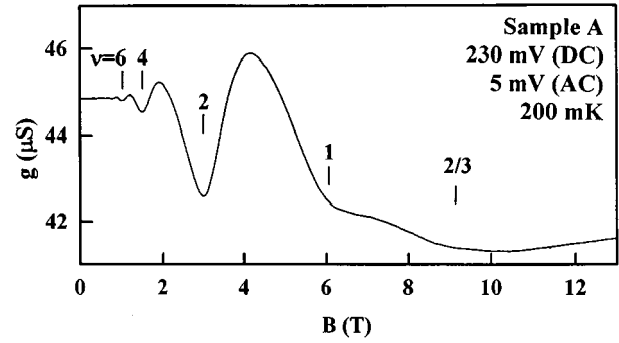


FIG. 6. Differential conductance (g) oscillations in magnetic field for sample A at a fixed bias of 230 mV at 200 mK.

the superconducting magnet, they clearly demonstrate an ability to access the extreme quantum limit with vertical transport. This work is continuing in a specially configured $^3\text{He}/^4\text{He}$ dilution refrigerator/60-T pulsed magnet system.

VI. CONCLUSION

In summary, we have studied resonant tunneling processes in double-well, triple-barrier heterostructures at low temperatures and in magnetic fields up to 48 T, demonstrating the critical influence of the second quantum well on charge accumulation in well 1 and thus on the overall tunneling characteristic. We identify two transitions specific to TBRTS's: GaAs LO-phonon emission assisted tunneling from the emitter to coupled well states in sample A, and a double resonance (elastic tunneling from the emitter to well 1 complemented by simultaneous GaAs LO phonon emission assisted tunneling from well 1 to well 2) in sample B resulting in significant enhancement of the tunneling current. We have demonstrated that the vertical tunneling current provides a probe of the ground state of a 2D electron system, having found evidence for a $\nu = \frac{2}{3}$ fractional quantum Hall effect state in oscillations of the peak current, and structure in $g(B)$ measurements in the extreme quantum limit.

ACKNOWLEDGMENT

We are indebted to P. E. Simmonds for many instructive discussions.

¹L. L. Chang, L. Esaki, and R. Tsu, Appl. Phys. Lett. **24**, 593 (1974).

²E. E. Mendez, L. Esaki, and W. I. Wang, Phys. Rev. B **33**, 2893 (1986).

³V. J. Goldman, D. C. Tsui, and J. E. Cunningham, Phys. Rev. Lett. **58**, 1256 (1987); T. C. L. G. Sollner, *ibid.* **59**, 1622 (1987).

⁴F. W. Sheard and G. A. Toombs, Appl. Phys. Lett. **52**, 1228 (1988).

⁵L. Eaves *et al.*, Solid-State Electron. **32**, 1101 (1989).

⁶T. J. Foster *et al.*, Phys. Rev. B **39**, 6205 (1989).

⁷W. I. E. Tagg *et al.*, Phys. Rev. B **48**, 4487 (1993).

⁸F. W. Sheard and G. A. Toombs, Semicond. Sci. Technol. **7**, B460 (1992).

⁹V. J. Goldman, D. C. Tsui, and J. E. Cunningham, Phys. Rev. B **36**, 7635 (1987).

¹⁰G. S. Boebinger *et al.*, Phys. Rev. Lett. **65**, 235 (1990).

¹¹M. L. Leadbeater *et al.*, Phys. Rev. B **39**, 3438 (1989).

¹²C. H. Yang, M. J. Yang, and Y. C. Kao, Phys. Rev. B **40**, 6272 (1989).

¹³P. J. Turley *et al.*, Phys. Rev. B **47**, 12 640 (1993).

- ¹⁴J. G. Chen *et al.*, Phys. Rev. B **43**, 4531 (1991).
- ¹⁵J. Leo and A. H. MacDonald, Phys. Rev. Lett. **64**, 817 (1990).
- ¹⁶T. Nakagawa *et al.*, Appl. Phys. Lett. **49**, 73 (1986).
- ¹⁷J. J. L. Rascol *et al.*, Phys. Rev. B **41**, 3733 (1990).
- ¹⁸H. Asahi *et al.*, Appl. Phys. Lett. **59**, 803 (1991).
- ¹⁹L. D. Macks *et al.*, Physica B **201**, 374 (1994).
- ²⁰P. M. Martin *et al.*, Semicond. Sci. Technol. **9**, 493 (1994).
- ²¹T. S. Turner *et al.*, Solid-State Electron. **37**, 721 (1994).
- ²²H. Kurata and H. Sakaki, Surf. Sci. **305**, 369 (1994).
- ²³D. Bertram *et al.*, Phys. Rev. B **50**, 17 309 (1994).
- ²⁴M. R. Deshpande *et al.*, in *Proceedings of the 11th International Conference on High Magnetic Fields in the Physics of Semiconductors*, edited by D. Heiman (World Scientific, Singapore, 1995), p. 562.
- ²⁵M. A. Reed *et al.*, Appl. Phys. Lett. **54**, 1256 (1989).
- ²⁶H. C. Liu, Appl. Phys. Lett. **53**, 485 (1988).
- ²⁷Denoted $e \rightarrow 1 \rightarrow 2$ (triple resonance) in a preliminary report on this work (Ref. 24).
- ²⁸C. Zhang *et al.*, Phys. Rev. Lett. **72**, 3397 (1994).
- ²⁹G. S. Boebinger *et al.*, Phys. Rev. B **47**, 16 608 (1993).